

RoboWalk: Explicit Augmented Human-Robot Dynamics Modeling for Design Optimization

S. Ali A. Moosavian, Mahdi Nabipour, Farshid Absalan, Vahdi Akbari

Center of Excellence in Robotics and Control,
Advanced Robotics & Automated Systems (ARAS) Lab, Department of Mechanical Engineering,
K. N. Toosi University of Technology, Tehran, Iran

Abstract

Utilizing orthoses and exoskeleton technology in various applications and medical industries, particularly to help elderly and ordinary people in their daily activities is a new growing field for research institutes. In this paper, after introducing an assistive lower limb exoskeleton (RoboWalk), the dynamics models of both multi-body kinematic tree structure human and robot is derived separately, using Newton's method. The obtained models are then verified by comparing the results with those of the Recursive Newton-Euler Algorithm (RNEA). These models are then augmented to investigate the RoboWalk joint torques, and those of the human body, and also the floor reaction force of the complete system. Since RoboWalk is an under-actuated robot, despite the assistive force, an undesirable disturbing force exerts to the human. So, optimization strategies are proposed to find an optimal design to maximize the assistive behavior of RoboWalk and reduce joint torques of the human body as a result. To this end, a human-model-in-the-loop optimization algorithm will be used. The solution of this optimization problem is carried out by Particle Swarm Optimization (PSO) method. The designed analysis and the optimization results demonstrate the effectiveness of the proposed approaches, leading to the elimination of disturbing forces, lower torque demand for RoboWalk motors and lower weights.

Keywords

Assistive exoskeleton, Dynamics modeling, Recursive Newton Euler Algorithm, Optimization, Particle Swarm Optimization, Floor reaction force

Introduction

Humanoid robots with highly nonlinear dynamics are systems with a high degree of freedom with multiple links. These robots are inherently unstable, so to control should be first dynamically stabilized¹. Lots of research has been performed on this field for different scenarios and surface conditions^{2, 3}. Human-robot rehabilitation technology is one of the spinoffs of humanoid technology where a part of the tasks is taken over by the human itself. Orthosis and exoskeletons are widely used in both medical industries for curing patients suffering from spinal cord injury⁴ and for strength augmentation in soldiers and workers. Robotic gait rehabilitation trainer⁵, Lokomat⁶, ALEX⁷, LOPES⁸, etc. are some examples of treadmill-based immobile exoskeletons. HAL⁹, National University of Singapore orthosis¹⁰, ReWalk¹¹, etc. are examples of portable rehabilitation exoskeletons. The BLEEX exoskeleton¹² of University of California, Berkeley is the most well-known exoskeleton of strength augmentation type. Robo-Knee¹³ and MIT augmentation exoskeleton¹⁴ are other types of these devices.

Another important class of wearable robots are assistive exoskeletons. The intention of using such groups of exoskeletons are assisting the weak elderly to become needless of walker, sticks or help of others in doing their daily activities¹⁵. In addition, it can help healthy users to do their tasks by spending less energy in longer periods of time. As for some examples of passive assistive exoskeletons, one can mention the, XPED2¹⁶, Passive Ankle Exoskeleton¹⁷, MoonWalker¹⁸. One of the most successful active assistive robots is the Honda bodyweight support assist device¹⁹. The elders, tourists, factory workers and, generally, people who should be on foot for hours are the main target society of this device. This device has an attractive design which includes a seat for the user that is placed under the groin region. Wearing the device is as easy as putting on the shoes and placing the seat under the user pelvis. The objective of the control strategy is to offer maximum reduction in felt weight in single support phase. The results showed a reduction of 10% of bodyweight (Floor Reaction Force, FRF) during mid stance phase. Unfortunately, this device produces an

unwanted horizontal force in frontal plane²⁰ which causes interruptions and may be a threat to user stability or may increase joint torques during the walking gait cycle. This is a big deficiency and in this paper this problem is addressed and somewhat resolved by structural optimization.

The design and function of this device has captured lot of attention. The passive Bodyweight support exoskeleton with compliant knee²¹ and assistive exoskeleton device fabricated in Ottawa University²² are examples of assistive devices inspired by Honda bodyweight support assist device. The former claims to reduce the knee joint torque up to 27% in some points of mid stance phase but although it uses a compliant knee, its design isn't optimized and it has bad influence on user gait. In the latter case, the kinematic results revealed that the device interrupts in the user gait. In addition, the robot doesn't assist the user in most of the gait cycle. In both cases, no optimizations were performed and this could be a source of these bad influences on user gait.

Dimensional optimization has lots of applications in robotic industries. Using genetic algorithm, dimensional synthesis is optimized for the working mechanism of a hydraulic excavator to improve the digging performance²³. Shim et al. has designed a robotic gripper for the front-end module assembly process and optimized a six-bar linkage by a multi-objective optimization approach²⁴. Pan et al. designed a scissor mechanism for load-carrying augmentation and the inverse dynamics was modeled by Kane's method²⁵. A non-model based Fuzzy-PID algorithm was simulated on the obtained model²⁶. Finally in ²⁷ a length optimization of the scissor sides to minimize the transmitting errors between the input and output motions in walking were performed. In another study, a passive upper limb exoskeleton was designed²⁸ and its elastic elements were optimized through a genetic algorithm.

In the field of lower limb exoskeleton, Kawale ²⁹ obtained the equations of motions by Lagrange method and performed optimization to achieve an energy efficient design for a wearable lower body exoskeleton mechanism in shipbuilding industry. Ortiz³⁰ used a starting point dependent Nelder-Mead method for optimizing the structure and parameters of a soft modular lower limb exoskeleton to make it energetically efficient. Random sampling within the parameter space was performed to prevent finding the local minima. In Wang et al. an optimization framework to obtain an efficient and lightweight combinations for Mindwalker series elastic joint was proposed³¹. None of the above-mentioned articles, used knee joint torque of the human dynamics model as a criterion for their optimization. This problem is going to be addressed in this paper, along with other key elements included in the optimization algorithm.

This paper lies in the continuity of previous works³²⁻³⁴ done in the context of modeling, design and performance analysis of RoboWalk exoskeleton. After a brief introduction to RoboWalk assistive exoskeleton structure and its functionality, the kinematics of RoboWalk is presented. The multi-body human user and exoskeleton are modeled by Newton's method, afterward. The modeling is performed in the sagittal plane, joints are assumed ideal³⁵ and all the analysis is conducted in single support phase (SSP). The models are then verified by modeling the human and robot using Recursive Newton Euler Algorithm. In the next step, in order to resolve the problem of the generated undesirable horizontal force that previous works suffered from, constrained dimensional optimization is executed using the PSO method. In this optimization problem, joint torques are used as a good criterion for analyzing user comfort and comparing RoboWalk influence before and after the optimization. Three optimization strategies consisting of a human-model-in-the-loop strategy with the goal of minimizing the disturbance force, user knee joint torque and RoboWalk motor torque are proposed and discussions are presented. Finally, the conclusions of this study are summarized in the last section.

Introducing RoboWalk Assistive Device

As mentioned before, the structure of RoboWalk is inspired of Honda's bodyweight support assist device which is explained in detail in ^{19, 33} and demonstrated in Figure 1.

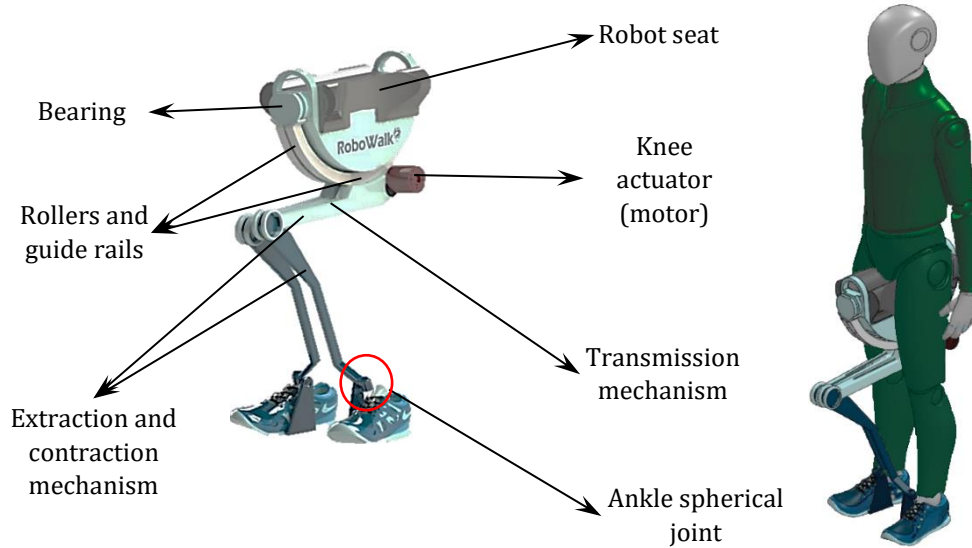


Figure 1. RoboWalk structure

The user wears the shoes of the device and, after turning the device on, raises the seat up to the groin area. It is worth noting that the legs of RoboWalk remain between the legs of the user during the entire gait. This is a beneficial design allowing the device to have low moment of inertia. The seat is designed intelligently to provide a 3-DOF rotational motion. the knee joint has 1-DOF in its sagittal plane and the ankle spherical joint permits a 3-DOF rotation. During simulations the robot seat is assumed to be stuck to user pelvis and the robot's ankle joint is fixed to user shoes. Hence, after the robot is set in place, RoboWalk kinematics is completely specified.

Integrated System Modeling

In this section, the kinematics and dynamics of the human body and RoboWalk are discussed. The procedure of deriving the EoMs of the system is depicted in figure 2 briefly.

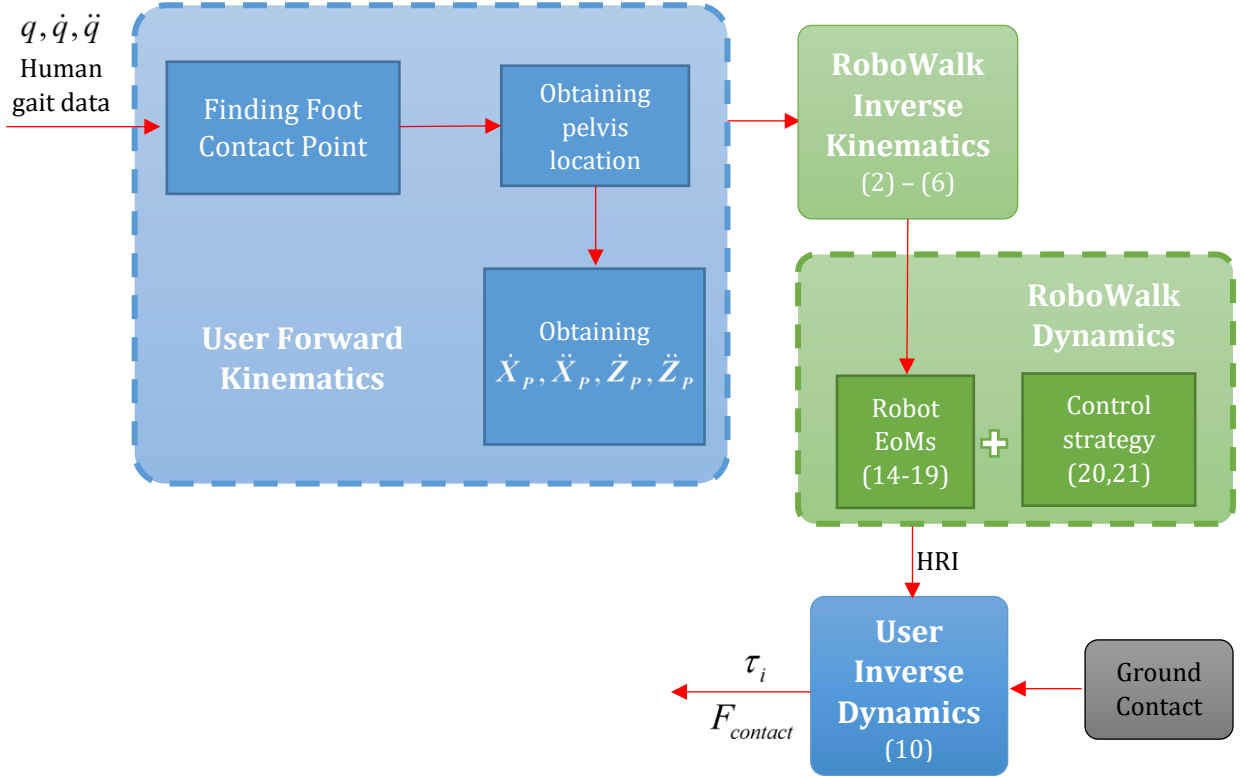


Figure 2. Procedure for deriving the EoMs of the system

X_p and Z_p are the pelvis coordinates in sagittal plane and q is human limb angles. The first task in obtaining user's forward kinematics is to find the foot contact point. This could be done by finding the maximum height between a reference point (e.g. pelvis) and toe/heel of the user and assigning the maximum amount as height of the reference point³³. Since the connection points of RoboWalk is invariant with respect to human body, by knowing the forward kinematics of user, the inverse kinematics of RoboWalk is easily obtained. As a result, the robot's inverse dynamics and hence its interaction with user is obtained. The human robot interaction (HRI) and the floor reaction force (FRF) are then assumed as external forces to the user inverse dynamics model. This procedure along with its governing equations is more discussed in subsequent sections.

Kinematics Modeling

In this section, the forward kinematics of human model and inverse kinematics of RoboWalk is obtained. The verification is performed in subsequent sections.

Human kinematic model

In this study, the human model is assumed to be an 8 linked multi-body system which includes pelvis, trunk, right and left thigh, shank and foot. The upper extremity is replaced by the trunk for ease in analysis. The pelvis is assumed to be the floating-base. Thus, the pose and orientation of the coordinate system attached to the center of pelvis is calculated with respect to the inertial coordinate system to allow movement analysis of the human user. The inertial coordinate system is located on the ground and under the user before starting to walk. All coordinate systems of this model are illustrated in Figure 3.

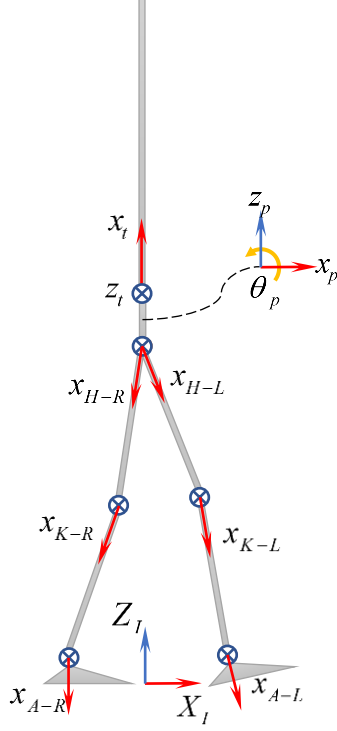


Figure 3. Coordinate systems used in the kinematics of user

In this figure, the arrows are the x-direction of coordinate frames and the crosses are those of z-direction. The vector of generalized coordinates that define the whole-body motion is specified as:

$$q = \begin{bmatrix} X_p & Z_p & q_p & q_t & q_h & q_k & q_a \end{bmatrix}^T \quad (1)$$

where X_p , Z_p and q_p the pose and orientation of pelvis reference coordinate with respect to inertia coordinate system, expressed in inertial reference. q_t , q_h , q_k and q_a represent the rotational motion of trunk, hip, knee and ankle joints for left and right legs. Since our analysis is restricted in sagittal plane, these joints represent 1-DoF revolute joints. By this definition, the human model is a 10-DoF kinematic tree structure in sagittal plane. The governing equations of human kinematics model are completely discussed in ³³.

RoboWalk Kinematic Model

As stated before, the robot interacts with the user in three points (both ankles and the seat). The directions of the forces applied to the seat are determined by kinematic relations. Consider the human and robot as shown in Figure 4.

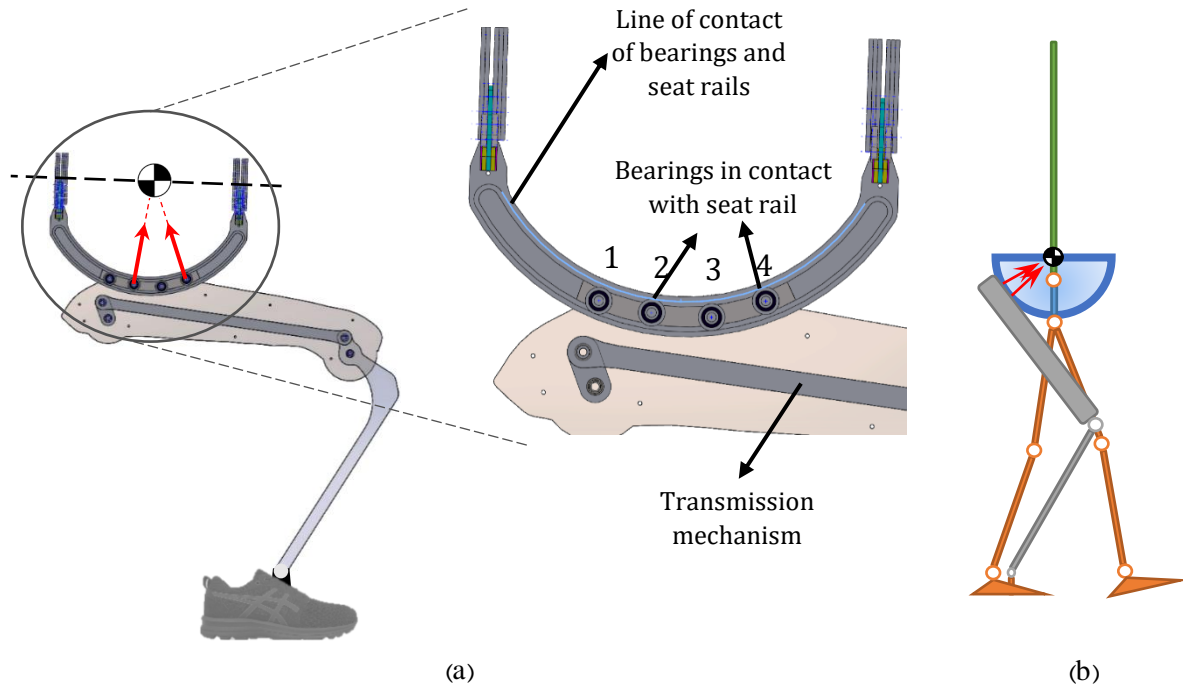


Figure 4. a) Force transmission to the user b) user and robot schematic

As shown in Fig. 4-a, wherever the bearings are in contact with the seat rails, a normal force is exerted to the rail (tangential friction force is neglected). This force is transmitted to the user through the seat. These rollers are stuck to the upper leg of the mechanism and are free to move in the guide rails. Rollers number 2 and 4 push the seat up and number 1 and 3 pull it down whenever needed. the forces exerted to the seat are directed toward the center of the guide arc (which is assumed to be almost coincident with the user's CoG). Fig. 4-b is a schematic of the user and one leg of the assistive robot and the direction of the assist force. Figure 5 demonstrates the important angles for introducing the kinematics of RoboWalk.

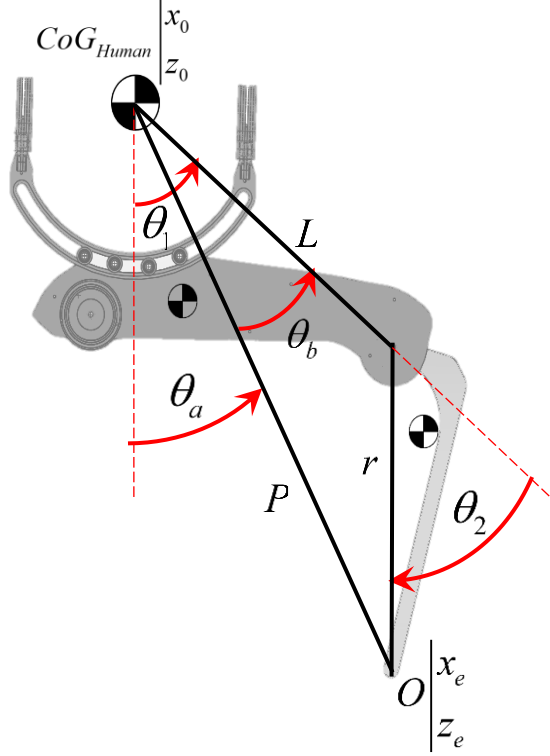


Figure 5. Kinematics of the robot

In this figure (x_0, z_0) is the center of guide rail arcs (i.e. approximate CoG of user) and (x_e, z_e) is the coordinate of robot ankle. The inverse kinematics of the robot in any configuration is as follow.

$$\theta_a = \tan^{-1} \left(\frac{x_e - x_0}{z_e - z_0} \right) \quad (2)$$

$$\theta_b = \cos^{-1} \left(\frac{L^2 + P^2 - r^2}{2LP} \right) \quad (3)$$

Since $\theta_1 = \theta_a + \theta_b$, the first link's angle with respect to vertical is known. By simple math operations θ_2 is obtained as follow.

$$\theta_2 = \cos^{-1} \left(\frac{P^2 - L^2 - r^2}{2Lr} \right) \quad (4)$$

By knowing the velocity and acceleration of (x_0, z_0) and (x_e, z_e) the link's angular velocities and accelerations are computed as follow.

$$\begin{bmatrix} \dot{\theta}_1 \\ \dot{\theta}_2 \end{bmatrix} = J^{-1} \begin{bmatrix} \dot{x}_e - \dot{x}_0 \\ \dot{z}_e - \dot{z}_0 \end{bmatrix} \quad (5)$$

$$\begin{bmatrix} \ddot{\theta}_1 \\ \ddot{\theta}_2 \end{bmatrix} = J^{-1} \left(\begin{bmatrix} \ddot{x}_e - \ddot{x}_0 \\ \ddot{z}_e - \ddot{z}_0 \end{bmatrix} - \dot{J} \begin{bmatrix} \dot{\theta}_1 \\ \dot{\theta}_2 \end{bmatrix} \right) \quad (6)$$

In this equation, J represents the jacobian of the robot ankle with respect to human's CoG.

Dynamics Modeling

After obtaining the kinematics relations of human model and RoboWalk, and possessing the gait data from Opensim software, the inverse dynamics relations can be acquired. As stated before, the FRF and HRI forces are the main external forces applied to the user. Hence, a general form of user dynamics is obtained and these external forces are then introduced to the equation. The general equation of a system when no constraints and external forces are applied to it is expressed as:

$$M(q)\ddot{q} + C(q, \dot{q}) = Q \quad (7)$$

in this equation, M represents a 10×10 inertia matrix. C and Q are 10×1 element vector. C represents Coriolis, centrifugal, gyration and gravity effects. Q is equivalent to $D\tau$ in the case when human is considered as a floating body with no interaction with environment. In this case, D and τ are defined as:

$$D = \begin{bmatrix} 0_{3 \times 7} \\ I_{7 \times 7} \end{bmatrix} \quad (8)$$

$$\tau = [0_{1 \times 3} \quad \tau_T \quad \tau_{HR} \quad \tau_{KR} \quad \tau_{AR} \quad \tau_{HL} \quad \tau_{KL} \quad \tau_{AL}]^T$$

in which τ_T is the joint torque of trunk, $\tau_{HR}, \tau_{KR}, \tau_{AR}$ are joint torques of right hip, knee and ankle and $\tau_{HL}, \tau_{KL}, \tau_{AL}$ are those of the left leg, respectively. Then, in order to include the external ground contact forces in the EoM, one could develop constrained dynamics model by simply replacing unknown forces/moments acting on the point of contact. The mapping of these forces to the space of generalized coordinates is carried out using the transpose of jacobian of the contact point. In this case, $Q = D\tau + J_{FRF}^T F_{contact}$ where J_{FRF} is the jacobian of contact point and $F_{contact}$ is the vector of external forces/moments exerted to that point. Thus, the EoM of the human model can be specified as:

$$M(q)\ddot{q} + C(q, \dot{q}) = D\tau + J_{FRF}^T F_{contact} \quad (9)$$

When RoboWalk is exploited, the HRI forces add to EoM as external forces. These HRI forces include the force exerted to the foot of the user by robot's ankle joint and the assisting forces applied to user's pelvis toward user CoG. Hence, the EoM of the augmented human-robot in SSP turns into the following equation.

$$\begin{bmatrix} \tau \\ F_{contact} \end{bmatrix}_{10 \times 1} = \begin{bmatrix} D & J_{FRF}^T \end{bmatrix}_{10 \times 10}^{-1} \begin{bmatrix} M(q)\ddot{q} + C(q, \dot{q}) - \\ -J_A^T F_A - J_{CoG}^T F_{CoG} \end{bmatrix} \quad (10)$$

where J_{CoG} and F_{CoG} are the jacobian of user's CoG and the known assistive forces obtained from robot inverse dynamics. In addition, in this equation

$$J_A^T F_A = J_{A_L} F_{A_L} + J_{A_R} F_{A_R} \quad (11)$$

In this equation, J_{A_L} and J_{A_R} are the robot's left and right ankle jacobian and F_{A_L} and F_{A_R} are the known forces exerted on RoboWalk ankle joint.

Since $\begin{bmatrix} D & J_{FRF}^T \end{bmatrix}$ is a square matrix, joint torques and contact forces are uniquely determined in SSP. In double support phase (DSP) the EoM is as follow.

$$M(q)\ddot{q} + C(q, \dot{q}) = D\tau + J_{FRF_L}^T F_{FRF_L} + J_{FRF_R}^T F_{FRF_R} \quad (12)$$

$J_{FRF_L}^T$ and $J_{FRF_R}^T$ represent the jacobian of the left and right foot contact points. In this case, the number of unknowns exceeds the number of EoMs by three (the simulation is conducted in sagittal plane) and the problem is solved by Minimum Norm method.

$$A^\dagger = A.(A^T A)^{-1} \quad (13)$$

As the RoboWalk is in its most extreme situation is the SSP, and the fact that DSP is a very short time in human gait, the DSP is excluded from our analysis.

Human-Body Dynamics model (Newton's Method)

The dynamics equation of a multi-body system (Equation (7)) can be obtained by two different approaches. In the first approach, internal forces are omitted from the EoM (e.g. Lagrange method). in the second approach, the internal forces in the EoM are explicitly included (e.g. Newton-Euler method). Since minimizing the human joint forces is one of the criteria of assessing the suitability of RoboWalk, Newton method is used for attaining the EoM of the entire system. The obtained multi-body system dynamics model is then verified using RNEA³⁶. In Figure 6, forces acting on user's shank and foot is shown.

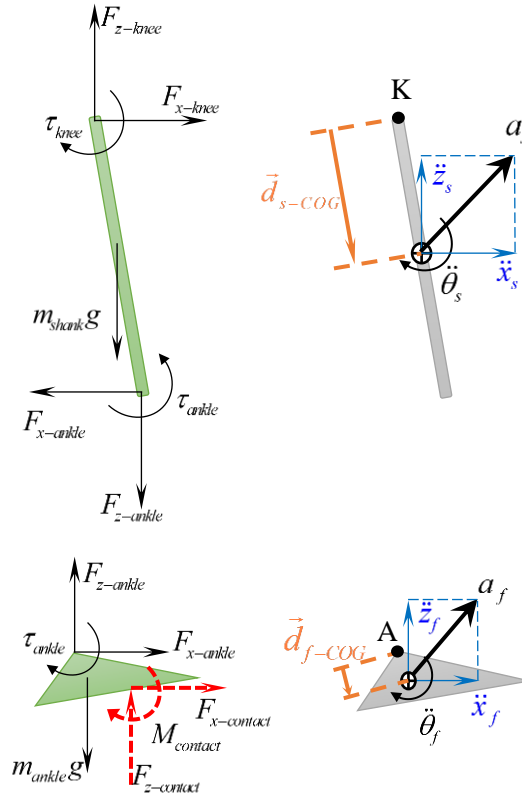


Figure 6. Free body diagram (FBD) and kinematic diagram of foot and shank

The contact forces $M_{contact}$, $F_{contact}$ are presented by dotted arrows. Foot EoM using Newton method is written as

$$\begin{aligned}
\sum F_x &= m_{foot} \ddot{x}_f \\
\sum F_z &= m_{foot} \ddot{z}_f \\
\sum M_A &= I_{foot} \ddot{\theta}_f + m_{foot} a_f \times d_{f-CoG}
\end{aligned} \tag{14}$$

Where, F_x , F_z and M_A are the forces and moment in ankle joint. m_{foot} and I_{foot} are foot mass and moment of inertia about foot CoG. \ddot{x}_f , \ddot{z}_f and $\ddot{\theta}_f$ are linear and angular acceleration of foot CoG. a_f and d_{f-CoG} represent foot CoG total acceleration and distance from ankle joint. The same is done for other limbs. The EoMs of human body limbs are gathered in appendix 1. In this way, all internal and external forces are included in the EoMs and a very comprehensive model is obtained. If the goal was to obtain an equation similar to Equation (7), the external forces should be neglected and, in addition, all internal reaction forces must be eliminated by substituting them by their kinematic values.

RoboWalk Dynamics Model (Newton's Method)

After obtaining the kinematics of RoboWalk, the device's dynamics equation is obtained by the same methods that human's dynamics were obtained. Figure 7 shows the FBD and kinematic diagram of the schematic assistive robot.

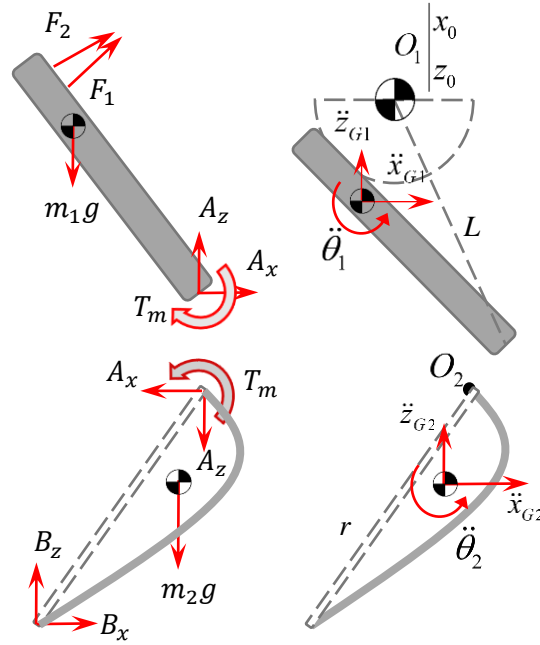


Figure 7. RoboWalk FBD and kinematic diagram in the sagittal plane

O_1 and O_2 are the center of rotation of upper and lower link respectively. Similar to the method for obtaining human model dynamics, three equations could be obtained for each link. Equations obtained for upper link are

$$F_1 \cos \alpha_{f_1} + F_2 \cos \alpha_{f_2} + A_x = m_1 \ddot{x}_{G1} \tag{15}$$

$$F_1 \sin \alpha_{f_1} + F_2 \sin \alpha_{f_2} + A_z - m_1 g = m_1 \ddot{z}_{G1} \tag{16}$$

$$m_1 g a + A_x L \cos \theta_1 + A_z L \sin \theta_1 + T_m = I_{G1} \ddot{\theta}_1 + m_1 (b \ddot{x}_{G1} - a \ddot{z}_{G1}) \tag{17}$$

where a and b are the horizontal and vertical distance between upper link CoG and human CoG (O_1) and L is the distance between RoboWalk knee joint and human CoG (O_1). The same is done for the lower link as follow

$$B_x - A_x = m_2 \ddot{x}_{G2} \quad (18)$$

$$B_z - A_z - m_2 g = m_2 \ddot{z}_{G2} \quad (19)$$

$$\begin{aligned} & B_x r \cos(\theta_1 + \theta_2) + B_z r \sin(\theta_1 + \theta_2) \\ & -T_m - m_2 g r_{G2} \sin(\theta_1 + \theta_2 + \beta) = I_{G2} (\ddot{\theta}_1 + \ddot{\theta}_2) \\ & + m_2 \ddot{x}_{G2} r_{G2} \cos(\theta_1 + \theta_2 + \beta) + m_2 \ddot{z}_{G2} r_{G2} \sin(\theta_1 + \theta_2 + \beta) \end{aligned} \quad (20)$$

where r_{G2} represent the distance between RoboWalk knee joint and lower link CoG. Hence, six equations are acquired for each leg of the robot.

Control Strategy. As it is illustrated in Figure. 8, there are seven unknown parameters (

$\vec{F}_1, \vec{F}_2, A_x, A_z, B_x, B_z$ and T_m) for each robot leg. Note that direction of \vec{F}_1 and \vec{F}_2 are known by knowing the kinematics of the robot. Hence, without introducing another equation to these 6 equations, finding an accurate solution to this problem is impossible.

To achieve this aim, a control strategy should be defined for the assistive exoskeleton. In this paper, the main purpose of using the device is to support a portion of the user's bodyweight and inducing the feeling of having less weight to the user. In order to do so, the objective of the robot leg that is in stance phase is to compensate a portion of the human's bodyweight. The other leg's actuator is assumed to be turned off. Hence, the 7th equation for the stance leg is going to be:

$$F_{z1} + F_{z2} = p \cdot W_{human} \quad (21)$$

in this equation, p represents the portion of the bodyweight that the robot supports. And for the leg that is in swing phase the 7th equation is:

$$T_m = 0 \quad (22)$$

By attaining these equations, all the unknown parameters are easily obtained in each sampling time.

Recursive Newton-Euler Algorithm (RNEA)

RNEA is a numerical approach to model the inverse dynamics. This algorithm is based on using 6×1 spatial coordinate³⁶ instead of the classical 3×1 representation³⁷ for each moment and force (or linear and angular velocity). Similar to classical NE method, all the equations are written in body coordinate. In Figure 8, forces acting on each body are shown.

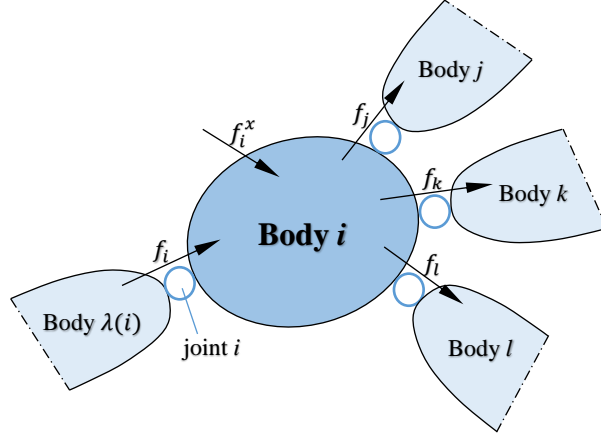


Figure 8. FBD of body i

In this figure, $\lambda(i)$ and f_i are the parent and the corresponding force exerted by it to body i . f_j, f_k, f_l are the forces applied by body i to bodies j, k and l . f_i^x represents the external force applied to body i by the environment. In this method, all external forces are considered as known values.

The equation of motion of a multi-body system in spatial coordinate is obtained by The spatial equation of motion states that the net force acting on a rigid body equals its rate of change of momentum³⁸:

$$f_i^B = \frac{d}{dt}(I_i v_i) = I_i a_i + v_i \times^* I_i v_i \quad (23)$$

in this equation, f_i^B represents the net force applied to i . The left side of this equation is the rate of change of body i 's angular momentum. \times^* , v_i, a_i and I_i are spatial force product sign, velocity, acceleration and moment of inertia, respectively. As illustrated in Figure 8:

$$f_i^B = f_i + f_i^x - \sum_{j \in \mu(i)} f_j \quad (24)$$

This equation is then reordered to obtain the recurrence relation of forces acting on body i :

$$f_i = f_i^B - f_i^x + \sum_{j \in \mu(i)} f_j \quad (25)$$

Equation (7) is solved by non-recursive algorithms, possessing a high computational complexity as $O(n^4)$. One the other hand, Recursive algorithms are much more efficient, possessing a computational complexities of $O(n)^{36}$. Hence, though non-recursive methods give preferable physical understanding, recursive algorithms are much better for implementation. Therefore, human and RoboWalk are modeled by RNEA and, for the sake of validation, the obtained results are compared with those of Newton's method in subsequent sections.

Structural Optimization

As mentioned in previous sections, each leg of RoboWalk assists the user by applying two forces toward the user CoG. The resultant of these two forces are two forces along X and Z direction in sagittal plane. Since RoboWalk has one actuator on each leg, it is an under-actuated system. As a result of this matter, one cannot possess control on setting both forces to a desired value. Hence, by assuming the control strategy

mentioned in equation (20), the assisting force in Z direction is set but the creation of the force applied to the user in X direction is inevitable. The effect of applying this horizontal force can be explained in such a way that the person is being pushed or pulled during walking and this probably makes inconvenience for the user.

This undesirable disturbing horizontal force could probably be vanished if the upper link of the robot could always be set to stay horizontal during the entire gait. In this way, most of the assisting force created by motors would remain in Z direction. For this purpose, either upper or lower link of the robot must have variable length. This could be done using another actuator or passive elements like springs for changing the robot link length. Many designs were checked and studied but they either increased the weight of the system or its complexity with no guarantee of the disturbing force reduction in the entire gait.

Another approach for decreasing this horizontal force is optimizing the dimensions of the robot such that the horizontal force is managed along with having low torque demands for RoboWalk motor. Trying to keep the motor torques low has two benefits. It permits using smaller and low power gears and motor and therefore, helps keeping robot's weight and manufacturing cost as low as possible. Hence, it is concluded that the cost function should be as follow.

$$J = \left| \sum F_x \right| + \left| \sum T_m \right| \quad (26)$$

In this equation, F_x and T_m represent horizontal force and motor torque, respectively. The design parameters are chosen to be L (distance between user CoG and RoboWalk knee), r (lower link length), R (arc radius) and θ_{opt} (angle between L and the line passing through human CoG and bearing applying force to the user) which are all circled in the Figure 9. The rest of the parameters are considered to be a function of $\begin{bmatrix} L & r & R & \theta_{opt} \end{bmatrix}^T$ parameter set.

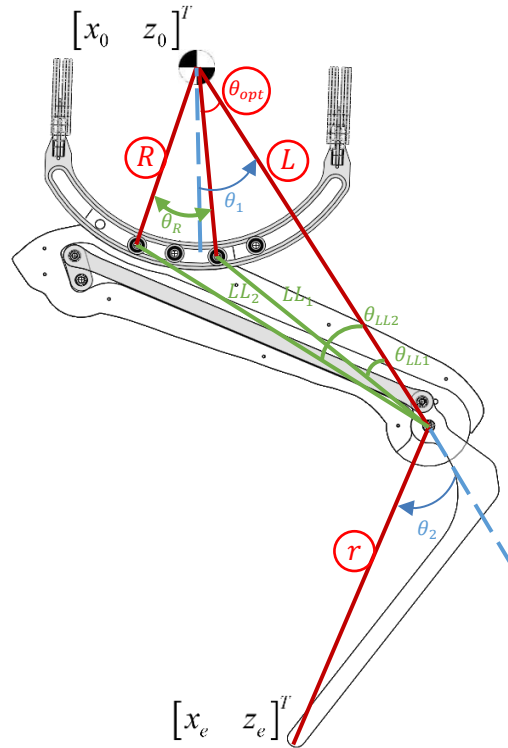


Figure 9. RoboWalk optimization parameters (circled parameters are directly obtained by optimization)

Three methods were examined to design RoboWalk optimally. Since this problem is a continuous optimization problem, PSO method is used to obtain the optimal parameter values for each robot leg. It is worth mentioning that this optimization process is a constrained optimization problem. All parameters are bounded, giving the set of inequality constrains as follow:

$$\lambda_i^{\min} \leq \lambda_i \leq \lambda_i^{\max} \quad (27)$$

when finding optimal parameters, the geometrical and velocity constraints shouldn't be violated. Some of these geometrical constraints are mentioned as.

$$x_0 + L \sin \theta_1 + r \sin(\theta_1 + \theta_2) = x_e \quad (28)$$

$$z_0 - L \cos \theta_1 - r \cos(\theta_1 + \theta_2) = z_e \quad (29)$$

$$\frac{\sin \theta_{opt}}{LL_1} = \frac{\sin \theta_{LL1}}{R} \quad (30)$$

$$\frac{\sin(\theta_{opt} + \theta_R)}{LL_2} = \frac{\sin \theta_{LL2}}{R} \quad (31)$$

a) First approach for structural optimization

In the first approach, optimization is conducted corresponding to each gait sample. In other words, when the user steps a single sample time forward, valid combinations (population) of parameter set values are chosen and the cost function is evaluated for each parameter set. Consecutive parameter sets are selected such that the cost function reduces in every step. In this approach the cost function is proposed as

$$J_1 = w_1 \left| \sum F_x \right| + w_2 \left| \sum T_m \right| + w_i \times \text{Geometrical constraints} \quad (32)$$

Where w_1 , w_2 and w_i are weights and F_x and T_m represent horizontal force exerted to user and RoboWalk motor torque, respectively. The horizontal force is obtained according to user posture and RoboWalk configuration for the intended parameter set. The structure of the optimization problem in the first approach is illustrated in Figure 10 as follow. As it is shown in the figure, the optimal parameters that minimize the cost function are obtained for every sample gait data (k^{th} gait sample).

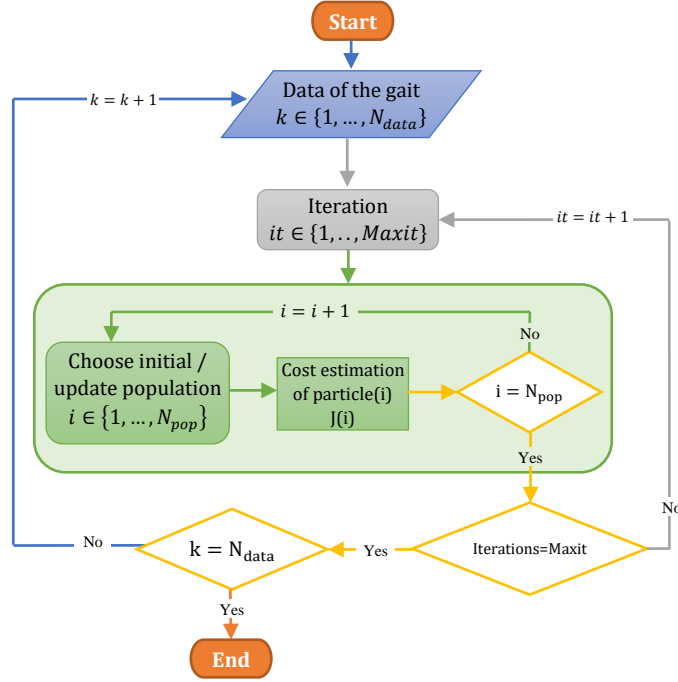


Figure 10. The first approach of optimization structure

In this figure, N_{data} is the number of data samples, N_{pop} is particle population (number of parameter sets) and Maxit is the number of iterations made for every gait sample to find the optimal structure for that gait sample.

b) Second approach for structural optimization

In this method, unlike the previous method that the optimization was done for every gait sample, the optimization is done for the entire gait at once. The structure of this optimization approach is depicted in Figure 11.

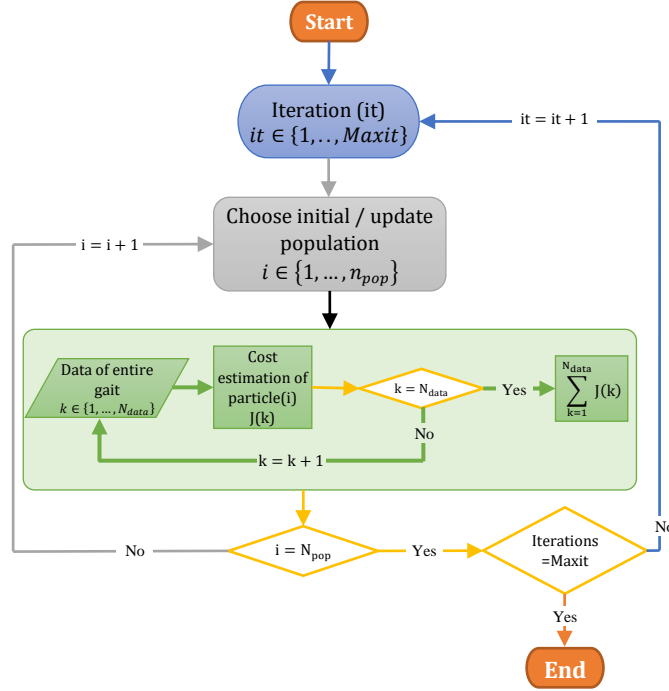


Figure 11. The second approach of optimization structure

In this structure, unlike the first approach that different parameter sets were chosen for every gait sample, a parameter set is chosen for every iteration and the cost is estimated for those parameters during the entire gait. Then, in the next iteration, another parameter set is selected and the cost estimation is performed once again. The estimated cost is the sum of all cost during each sample gait. The PSO algorithm that minimizes this cost function is capable of finding optimal structural parameters to minimize a cost over the entire gait cycle. The cost function in this approach is similar to the previous.

$$J_2 \Big|_{\text{gait sample}} = w_1 |F_x| + w_2 |T_m| + w_i \times \text{Geometrical constraints} \quad (33)$$

This cost function should be estimated for every set of parameters for the entire gait (every iteration). Hence, it must be added or averaged for each iteration (entire gait) as follow

$$J_2 \Big|_{\text{iteration (gait)}} = \sum_{i=1}^{N_{\text{data}}} \left\{ w_1 |F_x| + w_2 |T_m| + w_i \times \text{Geometrical constraints} \right\} \quad (34)$$

The only objection to this approach is that although it considers the horizontal force as the main contributing factor to the increase of knee joint torque, it doesn't involve the knee torque directly.

c) Human-model-in-the-loop method

The human model-in-the-loop method is proposed to overcome the problem of previous method. In this method, the dynamics of human model is involved in each cost function evaluation. The structure of this method is illustrated in Figure 12 as follow.

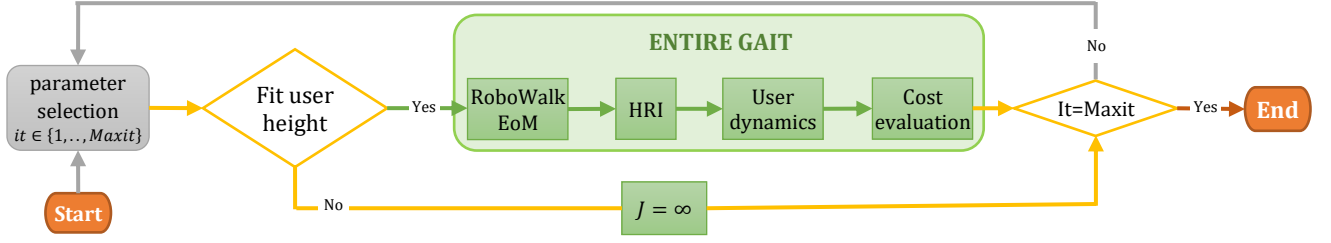


Figure 12. The optimization structure of the human-model-in-the-loop method

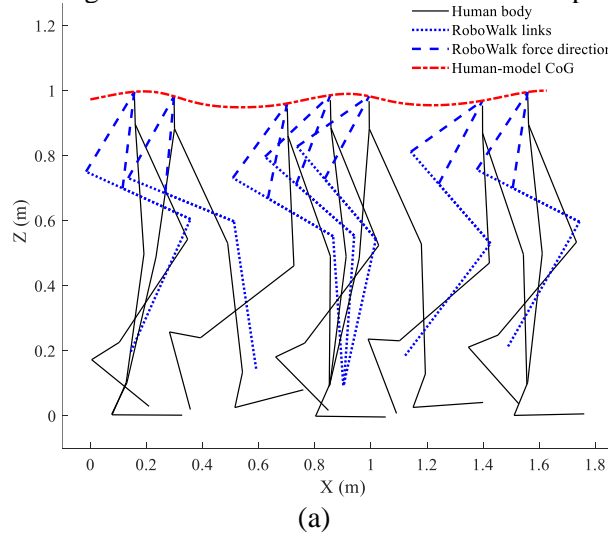
in the first step of this optimization method, random parameters are selected for the robot. These parameters are examined to fit for a specific user height. If the parameters selected couldn't fit the desired user, another set of parameters will be chosen. Otherwise, this set of parameters will be used for the robot in the entire gait. By knowing the kinematics of the user, RoboWalk kinematics will be estimated using the selected parameters. Knowing the kinematics leads to obtaining the forces applied to the user by the robot. The interaction between robot and user in every iteration cause different assisting forces and different knee torque as a result. Hence, the cost function to obtain the least knee torque for the user is as follow.

$$J_3 = \sum_{i=1}^{N_{data}} \left\{ w_1 |\tau_{knee}| + w_2 |T_{m_L}| + w_3 |T_{m_R}| + w_i \times \text{geometrical constraints} \right\} \quad (35)$$

In this cost function, τ_{knee} , T_{m_L} and T_{m_R} are the knee torque for each user leg, motor torque of left and right leg of RoboWalk, respectively. This cost function should be estimated for every set of parameters (every iteration). Hence, it must be added or averaged for each iteration (entire gait).

Obtained Results and Discussion

The kinematics of the augmented system is verified by Figure 13. In this figure the dotted line is the locus of human model CoG, the dotted-dashed line is the direction of assisting forces applied to the user (directed toward user CoG), bold solid lines are RoboWalk left leg expansion and contraction mechanism and thin solid line is lower extremity of human user. In order to verify the models, the Newton method is compared to the numerical RNEA. For arbitrary trajectories of the joints, joint forces are obtained by these methods and compared to each other. In Figure 13 the result of both methods is compared.



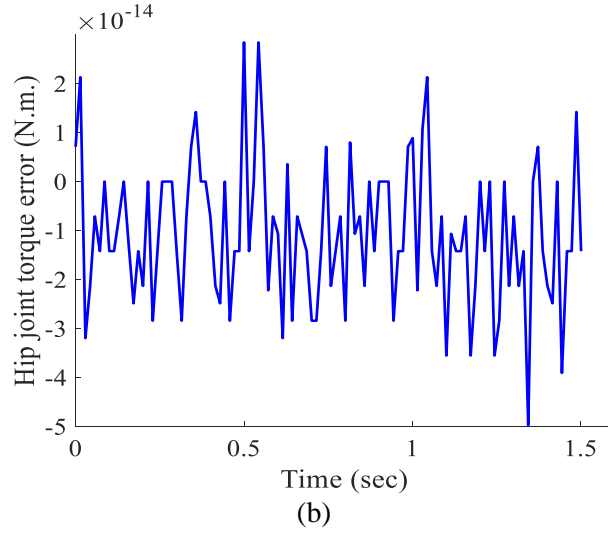


Figure 13. a) Kinematics verification and b) dynamics verification (error between Newton algorithm and RNEA) As it can be observed from this figure, both methods yield same results and the error between them (of the order of 10^{-14}) is due to computation round off. Tables 1 and 2 illustrate human and robot's mass properties and geometrical specifications. Human's specifications were obtained from the human model in Opensim software and the robot's specifications are intuitively chosen regarding Honda's bodyweight support system. It should be noted that Honda's robot total weight is 6.5 Kg and we decided to assume it to be 8 Kg in a conservative estimation.

Table 1. Human and RoboWalk mass properties

| Link | Mass (Kg) |
|-----------------------|-----------|
| Foot | 1.56 |
| Shank | 3.7 |
| Thigh | 9.3 |
| Pelvis | 11.78 |
| Trunk | 34.24 |
| Robot upper link mass | 3 |
| Robot lower link mass | 1 |
| Human total weight | 75.14 |
| Total robot weight | 8 |

The geometric properties of human and RoboWalk is as follows.

Table 2. Human and RoboWalk geometrical properties

| Link | Length (cm) |
|------------------------------------|-------------|
| Foot | 25 |
| Ankle joint height from the ground | 10 |
| Shank | 40 |
| Thigh | 40 |
| Pelvis | 17 |
| Trunk | 60 |
| Robot upper link | 55 |
| Robot lower link | 55 |

| | |
|---|----|
| Horizontal distance of robot ankle with respect to human ankle | 5 |
| Vertical distance of robot ankle with respect to human ankle | 0 |
| Circle arc radius | 20 |

Using these geometrical and mass specifications and obtaining the kinematic gait data from Opensim software, the RoboWalk influence on user's knee force are shown in Figure 14 the solid and dashed line is after and before using RoboWalk, respectively.

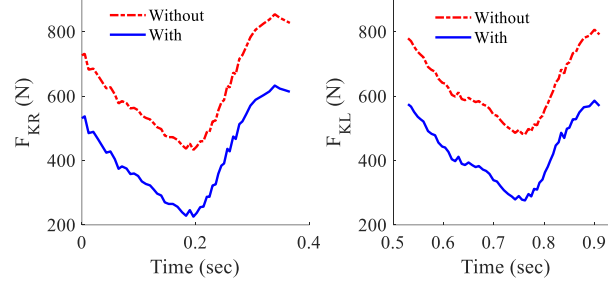


Figure 14. Right and left knee force with and without RoboWalk

In this figure, F_{KR} and F_{KL} represent joint force of right and left knee, respectively. Elders are mostly vulnerable at knee joints due to weak muscles and arthritis. In patients suffering from knee arthritis, the force exerted on knee causes pain. It is demonstrated in this figure that the joint force has decreased dramatically after utilizing RoboWalk. Simulations showed an increase in joint torques after using the device in most of the gait cycle. This is an important fact which could harass and exhaust the user. Hence, it can be concluded that most of the force is tolerated by the muscles and the bone on bone forces reduced considerably. The increased joint torque is due to the horizontal force exerted by the robot to the user. To overcome this problem, we can either reduce the percentage of RoboWalk assisting force or change the structure such that the horizontal force decreases. Accordingly, a structural optimization with the goal of minimizing user knee joint torque and robot motor torque is conducted.

Structural Optimization

Due to the underactuated nature of RoboWalk, an undesirable horizontal force is generated simultaneous with the vertical assistance force. The effect of this force on user's knee joint is minimized by optimizing robot's dimensional specifications by the methods explained in previous chapter.

First approach

The optimization is conducted for 54 data samples when the left foot is in SSP. The following results were achieved by this method.

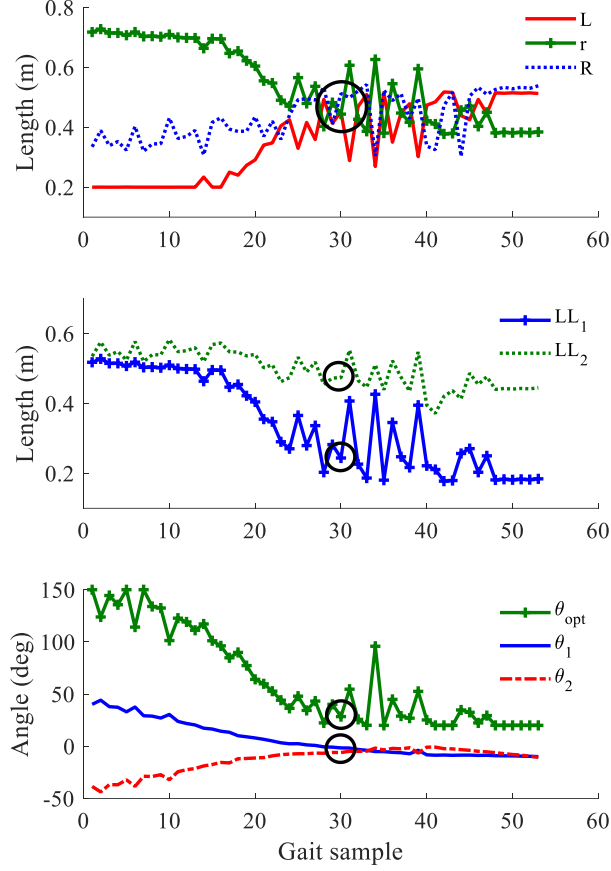


Figure 15. Optimized parameters obtained by the first approach
In this case, the force and robot motor torque are shown in Figure 16.

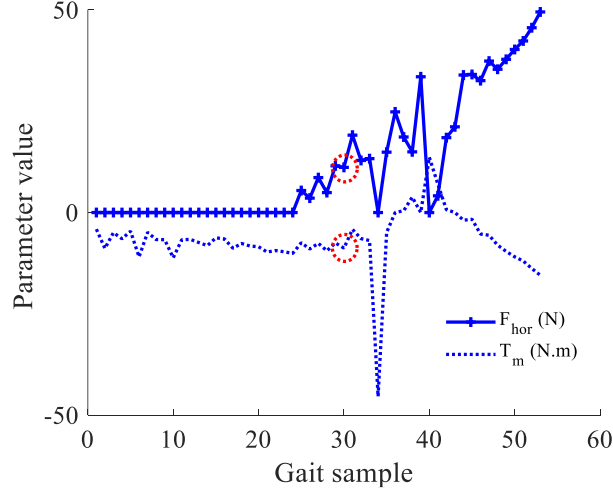


Figure 16. RoboWalk motor torque and the horizontal force applied to the user in the first approach

As it is demonstrated in Figure 16 in the first half of SSP, the average values of all parameters are different from the average values of the other half. Gait sample number 30 could be assumed as a suitable average sample for all parameters. Accordingly, good results for this optimization approach are summarized in table 3.

Table 3. Parameters obtained after optimization by the first approach

| parameter | L | r | R | LL ₁ | LL ₂ |
|-----------|---|---|---|-----------------|-----------------|
|-----------|---|---|---|-----------------|-----------------|

| | | | | | |
|---------------|----------------|------------|------------|-----------|-------|
| Average value | 0.45 | 0.45 | 0.51 | 0.24 | 0.47 |
| parameter | θ_{opt} | θ_1 | θ_2 | F_{hor} | T_m |
| Average value | 28.4 | -1.6 | -6 | 11.1 | -8.8 |

This approach benefits of its low calculation time for solving the optimization problem but unfortunately there is no precise optimal value for entire gait and an average value should be considered. There is no guarantee that the selected average value is an appropriate value for the rest of the gait.

Second approach

The optimization in this method is performed in the same situation as the previous. namely, the data samples and bounding of parameters are the same in both methods. Results of this optimization is illustrated in Figure 17 as follow.

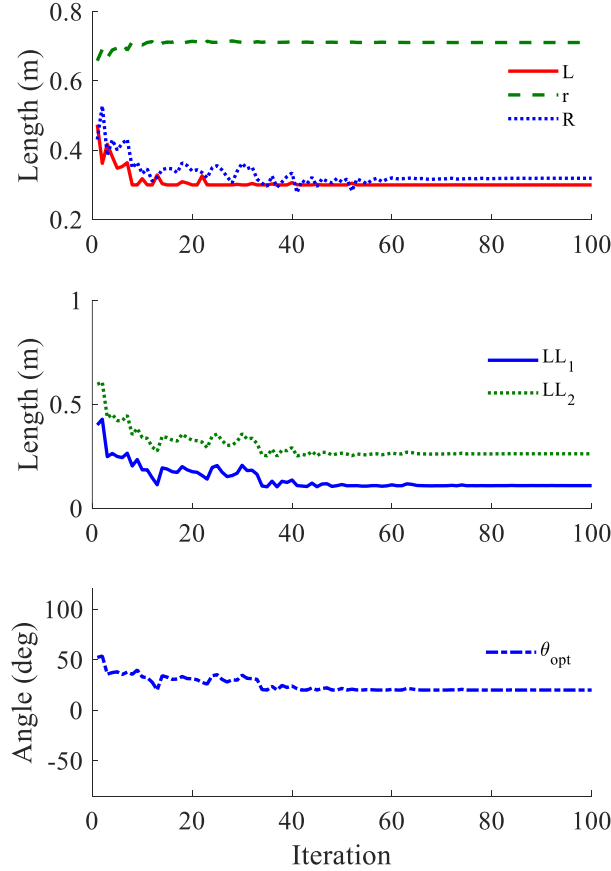


Figure 17. Optimized parameters obtained by the second approach

In this case, the force and robot motor torque are demonstrated in Figure 18.

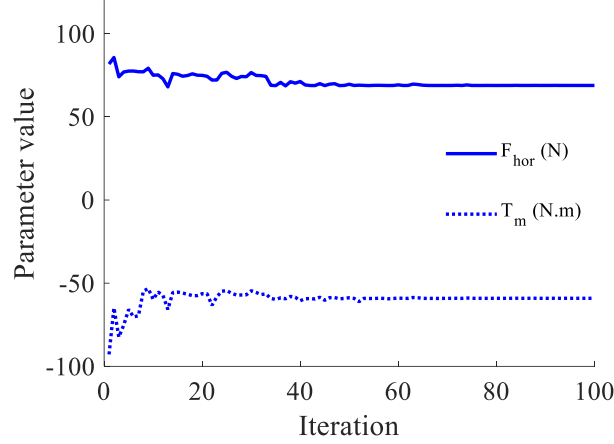


Figure 18. RoboWalk motor torque and horizontal force applied to the user in the second approach
As it is shown in these figures, robot parameters have converged to specific values. These values are optimized throughout the entire SSP and are reliable to produce the least horizontal force by using the least motor torque value. The parameter values after convergence of the algorithm is specified in table 4.

Table 4. Parameters obtained after optimization by the second approach

| parameter | L | r | R | LL ₁ |
|---------------|-----------------|----------------|------------------|-----------------|
| Average value | 0.3 | 0.71 | 0.32 | 0.11 |
| parameter | LL ₂ | θ_{opt} | F _{hor} | T _m |
| Average value | 0.26 | 20 | 69 | -59 |

The calculation time of this approach is less than the previous and the parameters converge to the values that minimize the overall cost function. The only deficiency of this approach is that it only deals with motor torque and horizontal force and it doesn't include the user knee joint actuation torque in the cost function. This problem is addressed in the next approach. In addition, LL₁= 11cm means that the distance between knee joint of RoboWalk and the seat is approximately 11cm. Which could cause problem when the user intends to sit or crouch. Since there is no control on LL₁ and LL₂ and they are attained by geometrical constraints, this could be considered as another drawback of this approach.

Human-model-in-the-loop

This method is suggested to solve the problems and deficiencies of previous methods. In this method, both motors torque and knee joint torque of human model is involved. Results of dimensional optimization for this approach is demonstrated in Figure 19.

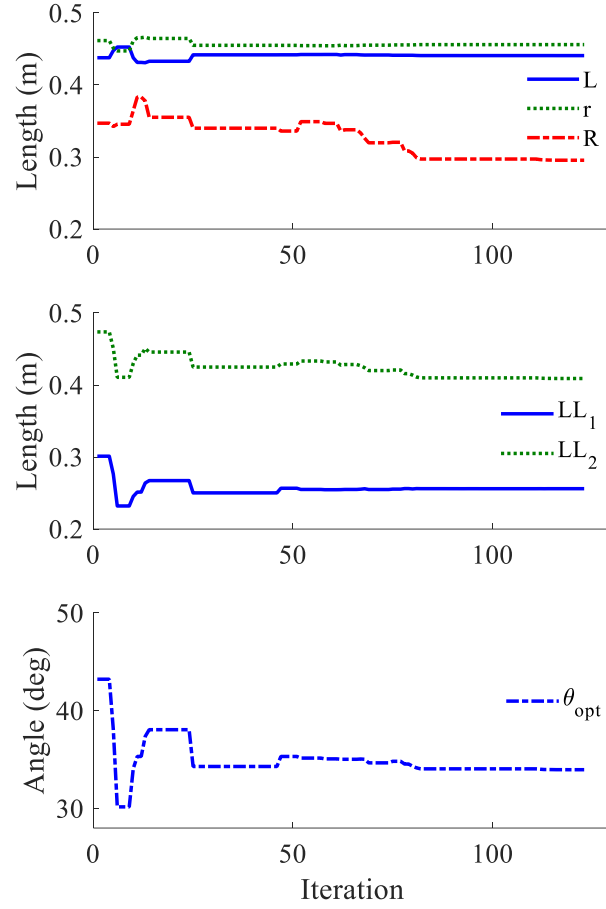


Figure 19. Optimized parameters obtained by the human-model-in-the-loop method
The parameter values after convergence of the algorithm is specified in table 5.

Table 5. Parameters obtained after optimization by the human-in-the-loop approach

| parameter | L | r | R | LL ₁ | LL ₂ | θ_{opt} |
|---------------|------|------|-----|-----------------|-----------------|----------------|
| Average value | 0.44 | 0.46 | 0.3 | 0.26 | 0.4 | 34 |

Using these optimal parameters, user knee joint torque is obtained and illustrated in Figure 20.

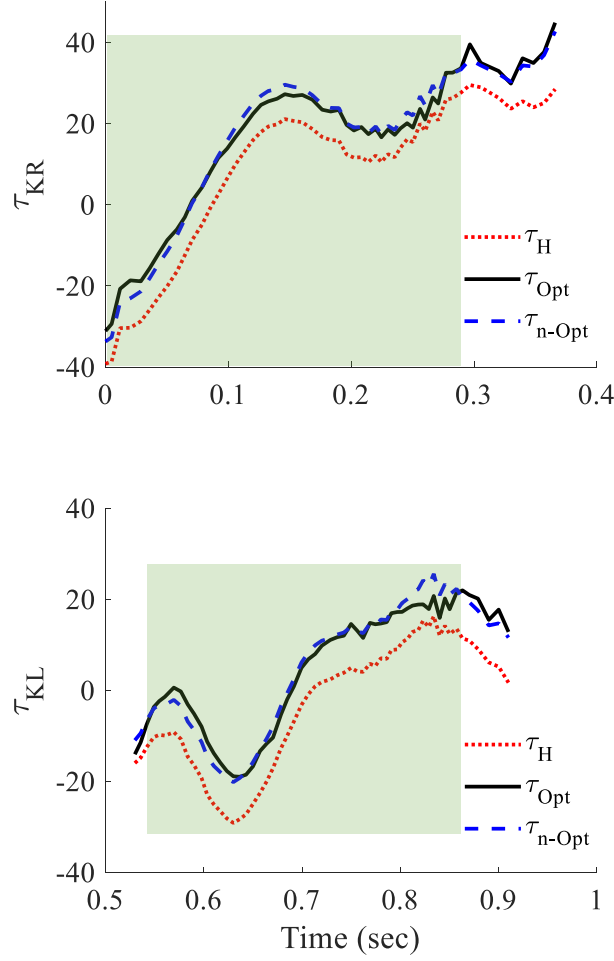


Figure 20. The user knee joint torque with and without RoboWalk (before and after optimization)

In this figure, the solid line is the joint torque obtained after using the optimal values, the dashed line is the user joint torque obtained after using the intuitive values (non-optimal joint torque) and the dotted line is human joint torque before utilizing RoboWalk. The hatched part of the plot is the area that the user joint is improved by using optimal values. Figure 21 depicts the speed-torque diagram of RoboWalk motors before and after optimization.

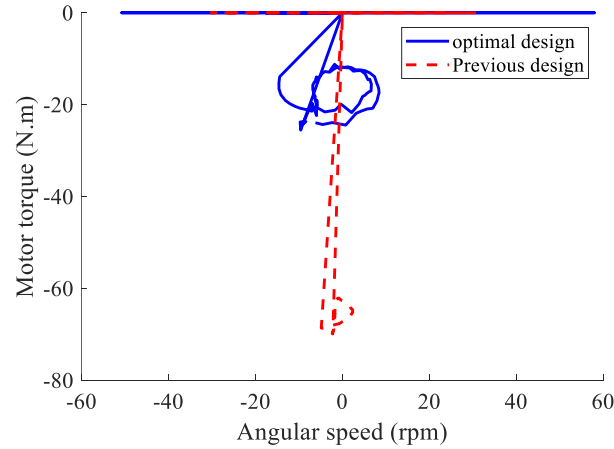


Figure 21. Speed-torque diagram of the motors before and after optimization in SSP (the torques in DSP are set to zero)

In previous design, RoboWalk motor should fulfill the requirement of 70N.m nominal torque in approximately 6rpm. It is shown that after optimization a 25 N.m. nominal torque in approximately 15rpm motor is enough. As a result of this valuable achievement, the required motor and gearbox for this design is lighter, more likely to be back-drivable and even more affordable in price. Which means the 630 grams EC 90 flat Ø90 mm, brushless, 360 W, with Hall sensors which delivers a nominal torque of 953mNm in nominal speed of 2340rpm along with a 30:1 gearbox is a very conservative and suitable selection for RoboWalk motor. This selection is far from good since it is even lighter than what we expected and used in our simulations for RoboWalk upper link mass (table 1).

Conclusions and Discussion

In this research, a lower limb assistive exoskeleton, named RoboWalk, was presented and its operational strategy was explained in detail. After modeling and verifying the kinematics and dynamics of this multi-body system, a control strategy was applied and RoboWalk performance and its effect on the user were investigated. The results showed that the robot reduces the felt bodyweight of the user by 33% using a 70 N.m. motor in approximately 6 rpm angular velocity but applied an unwanted disturbing horizontal force to the user which we have interpreted it as an extra torque load on the user's knee joint in some points of SSP. In order to overcome this problem, dimensional optimization was performed using different strategies by PSO algorithm. The results of these strategies are summarized in Table 6.

Table 6. Comparison of different optimization methods

| | First method | Second method | Human-model-in-the-loop method |
|--|---------------------|----------------------|---------------------------------------|
| Convergence | - | + | + |
| User comfort after optimization | Low | Moderate | High |
| RoboWalk motor torque after optimization | High | Moderate | Low |
| Overall system weight | Moderate | Moderate | Low |
| Computational time | Low | Very Low | High |

According to the simulations, the human-model-in-the-loop optimization strategy was found to be more useful than others. Two significant benefits of the human-model-in-the-loop optimization are that in addition to the fact that the user felt less disturbing joint torques, the motor's required specifications decreased such that not only the system gets lighter and cheaper, but it also remains in the region of back-drivability which is essential for user safety. In addition, selecting a lightweight motor leads to less disturbing forces for the user, for the leg in the swing phase. Thus, the human-model-in-the-loop method proved its efficiency. It is worth noting that this optimization strategy could be used for other exoskeletons or other human models, such as human models in Opensim or Anybody modeling systems.

References

1. Moosavian SAA, Alghooneh M and Takhmar A. *Cartesian Approach for Gait Planning and Control of Biped Robots on Irregular Surfaces*. 2011.

2. Ezati M, Khadiv M and Moosavian SAA. An Investigation on the Usefulness of Employing a Two-Segment Foot for Traversing Stairs. *I J Humanoid Robotics* 2017; 14: 1-31. DOI: 10.1142/S021984361750027X.
3. Khadiv M, Moosavian SAA, Yousefi-Koma A, et al. Online adaptation for humanoids walking on uncertain surfaces. *Proceedings of the Institution of Mechanical Engineers, Part I: Journal of Systems and Control Engineering* 2017; 231: 245-258. DOI: 10.1177/0959651817692484.
4. Lúgrís U, Carlín J, Luaces A, et al. Gait analysis system for spinal cord-injured subjects assisted by active orthoses and crutches. *Proceedings of the Institution of Mechanical Engineers, Part K: Journal of Multi-body Dynamics* 2013; 227: 363-374. DOI: 10.1177/1464419313494935.
5. Pietrusinski M, Cajigas I, Severini G, et al. Robotic Gait Rehabilitation Trainer. *IEEE/ASME Transactions on Mechatronics* 2014; 19: 490-499. DOI: 10.1109/tmech.2013.2243915.
6. Colombo G, Joerg M, Schreier R, et al. Treadmill training of paraplegic patients using a robotic orthosis. *J Rehabil Res Dev* 2000; 37: 693-700. 2001/04/26.
7. Banala SK, Kim SH, Agrawal SK, et al. Robot assisted gait training with active leg exoskeleton (ALEX). *IEEE Trans Neural Syst Rehabil Eng* 2009; 17: 2-8. 2009/02/13. DOI: 10.1109/TNSRE.2008.2008280.
8. Veneman JF, Kruidhof R, Hekman EE, et al. Design and evaluation of the LOPES exoskeleton robot for interactive gait rehabilitation. *IEEE Trans Neural Syst Rehabil Eng* 2007; 15: 379-386. 2007/09/27. DOI: 10.1109/TNSRE.2003.818185.
9. Kawamoto H and Sankai Y. Power Assist System HAL-3 for Gait Disorder Person. In: Berlin, Heidelberg, 2002, pp.196-203. Springer Berlin Heidelberg.
10. Chen G, Qi P, Guo Z, et al. Mechanical design and evaluation of a compact portable knee-ankle-foot robot for gait rehabilitation. *Mechanism and Machine Theory* 2016; 103: 51-64. DOI: 10.1016/j.mechmachtheory.2016.04.012.
11. Díaz I, Gil JJ and Sánchez E. Lower-Limb Robotic Rehabilitation: Literature Review and Challenges. *Journal of Robotics* 2011; 2011: 11. DOI: 10.1155/2011/759764.
12. Zoss AB, Kazerooni H and Chu A. Biomechanical design of the Berkeley lower extremity exoskeleton (BLEEX). *IEEE/ASME Transactions on Mechatronics* 2006; 11: 128-138. DOI: 10.1109/TMECH.2006.871087.
13. Pratt JE, Krupp BT and Morse CJ. The RoboKnee: an exoskeleton for enhancing strength and endurance during walking. *Proceedings - IEEE International Conference on Robotics and Automation* New Orleans. LA: Proceedings of the 2004 IEEE, 2004, p. 2430-2435.
14. Walsh CJ, Endo K and Herr H. A Quasi-Passive Leg Exoskeleton for Load-Carrying Augmentation. *International Journal of Humanoid Robotics* 2007; 4: 20. 506. DOI: 10.1142/S0219843607001126.
15. Taghvaei S, Tavasoli A, Feizi N, et al. A control-oriented dynamic model for sit-to-stand motion with fixed support. *Proceedings of the Institution of Mechanical Engineers, Part K: Journal of Multi-body Dynamics* 2018; 232: 265-273. DOI: 10.1177/1464419317731059.
16. Dijk Wv and Kooij HVd. XPED2: A Passive Exoskeleton with Artificial Tendons. *IEEE Robotics & Automation Magazine* 2014; 21: 56-61. DOI: 10.1109/MRA.2014.2360309.
17. Collins SH, Wiggin MB and Sawicki GS. Reducing the energy cost of human walking using an unpowered exoskeleton. *Nature* 2015; 522: 212. DOI: 10.1038/nature14288.

18. Krut S, Benoit M, Dombre E, et al. MoonWalker, a lower limb exoskeleton able to sustain bodyweight using a passive force balancer. In: *2010 IEEE International Conference on Robotics and Automation* 3-7 May 2010 2010, pp.2215-2220.
19. Ikeuchi Y, Ashihara J, Hiki Y, et al. Walking assist device with bodyweight support system. *Proceedings of the 2009 IEEE/RSJ international conference on Intelligent robots and systems*. St. Louis, MO, USA: IEEE Press, 2009, p. 4073-4079.
20. Jun Ashihara W, Yoshihisa Matsuoka T, Hiroshi Matsuda W, et al. *Walking Assist Device*. Patent US 9,161,880 B2, Japan, 2015.
21. Lee K and Wang D. Design analysis of a passive weight-support lower-extremity-exoskeleton with compliant knee-joint. In: *2015 IEEE International Conference on Robotics and Automation (ICRA)* 26-30 May 2015 2015, pp.5572-5577.
22. Lovrenovic Z. *Development and Testing of Passive Walking Assistive Exoskeleton with Upward Force Assist*. University of Ottawa, Faculty of Graduate and Postdoctoral Studies, 2017.
23. Zou Z, Chen J and Pang X. Optimum dimensional synthesis for the working mechanism of a hydraulic excavator to improve the digging performance. *Proceedings of the Institution of Mechanical Engineers, Part K: Journal of Multi-body Dynamics* 2018; 232: 357-370. DOI: 10.1177/1464419317736675.
24. Shim M and Kim J-H. Design and optimization of a robotic gripper for the FEM assembly process of vehicles. *Mechanism and Machine Theory* 2018; 129: 1-16. DOI: 10.1016/j.mechmachtheory.2018.07.006.
25. Pan D, Gao F and Miao Y. Dynamic research and analyses of a novel exoskeleton walking with humanoid gaits. *Proceedings of the Institution of Mechanical Engineers, Part C: Journal of Mechanical Engineering Science* 2014; 228: 1501-1511. DOI: 10.1177/0954406213509611.
26. Pan D, Gao F, Miao Y, et al. Bio-inspired control research of a novel lower extremity exoskeleton with a series-parallel mechanism. *Proceedings of the Institution of Mechanical Engineers, Part C: Journal of Mechanical Engineering Science* 2015; 229: 2875-2889. DOI: 10.1177/0954406214566036.
27. Miao Y, Gao F and Pan D. Prototype design and size optimization of a hybrid lower extremity exoskeleton with a scissor mechanism for load-carrying augmentation. *Proceedings of the Institution of Mechanical Engineers, Part C: Journal of Mechanical Engineering Science* 2015; 229: 155-167. DOI: 10.1177/0954406214532078.
28. Zhou L, Li Y and Bai S. A human-centered design optimization approach for robotic exoskeletons through biomechanical simulation. *Robotics and Autonomous Systems* 2017; 91: 337-347. DOI: 10.1016/j.robot.2016.12.012.
29. Kawale SS and Sreekumar M. Design of a Wearable Lower Body Exoskeleton Mechanism for Shipbuilding Industry. *Procedia Computer Science* 2018; 133: 1021-1028. DOI: 10.1016/j.procs.2018.07.073.
30. Ortiz J, Poliero T, Cairoli G, et al. Energy Efficiency Analysis and Design Optimization of an Actuation System in a Soft Modular Lower Limb Exoskeleton. *IEEE Robotics and Automation Letters* 2018; 3: 484-491. DOI: 10.1109/LRA.2017.2768119.
31. Wang S, Meijneke C and Kooij H. *Modeling, design, and optimization of Mindwalker series elastic joint*. 2013, p.1-8.
32. Moosavian SAA, Mohamadi MR and Absalan F. Augmented Modeling of a Lower Limb Assistant Robot and Human Body. In: *2018 6th RSI International Conference on Robotics and Mechatronics (IcRoM)* 2018, pp.337-342. IEEE.

33. Nabipour M and Moosavian SAA. Dynamics Modeling and Performance Analysis of RoboWalk. In: *2018 6th RSI International Conference on Robotics and Mechatronics (IcRoM)* 23-25 Oct. 2018, pp.445-450.
34. Nasrabadi AAM, Absalan F and Moosavian SAA. Design, kinematics and dynamics modeling of a lower-limb walking assistant robot. In: *2016 4th International Conference on Robotics and Mechatronics (ICROM)* 2016, pp.319-324. IEEE.
35. Shabana AA, Gantoi FM and Brown MA. Integration of finite element and multibody system algorithms for the analysis of human body motion. *Procedia IUTAM* 2011; 2: 233-240. DOI: 10.1016/j.piutam.2011.04.022.
36. Featherstone R. *Rigid Body Dynamics Algorithms*. 1 ed.: Springer US, 2008, p.272.
37. Craig JJ. *Introduction to Robotics: Mechanics and Control*. Pearson/Prentice Hall, 2005.
38. Siciliano B and Khatib O. *Springer Handbook of Robotics*. Springer International Publishing, 2016.

Appendix

Notation

| | |
|-----------------|--|
| a_i | Spatial acceleration |
| A_x, A_z, T_m | RoboWalk knee joint forces and torque |
| B_x, B_z | Forces in RoboWalk ankle |
| d_{f-CoG} | Distance between ankle joint and foot's CoG |
| d_{s-CoG} | Distance between knee joint and shank's CoG |
| f_i^x | External force exerted on body i |
| F | External (foot contact) force |
| F_1, F_2 | Forces applied to user by RoboWalk |
| $F_{contact}$ | Force applied to the foot |
| F_x | Horizontal force exerted to the human user |
| G | Matrix of gravity effect |
| J | Jacobian matrix |
| L | The magnitude of line drawn between RoboWalk knee and user CoG |
| LL_1, LL_2 | The magnitude of line drawn between RoboWalk knee and first and second bearing |
| $M(q)$ | Mass matrix |
| m_1, m_2 | upper and lower link of RoboWalk |
| $M_{contact}$ | Moment applied to the foot |
| p | Portion of the bodyweight that the robot supports |

| | |
|------------------------------|--|
| q_p | rotational motion of pelvis with respect to the inertia. |
| q_t, q_h, q_k, q_f | rotational motion of trunk, hip joints and knee joints with respect to the parent limb |
| R | RoboWalk seat arc radius |
| T_{m_L}, T_{m_R} | Left and right RoboWalk motor torques |
| v_i | Spatial velocity |
| V | Matrix of Coriolis and centrifugal and gyration effect |
| (x_0, z_0) | Approximate CoG of user |
| (x_e, z_e) | Coordinate of robot ankle |
| X_p, Z_p | pelvis reference frame movements with respect to inertia frame |
| <i>Greek symbols</i> | |
| $\alpha_{f_1}, \alpha_{f_2}$ | RoboWalk assistive force angles with respect to horizon |
| τ | Human joint torque |
| λ | Parent |
| θ_1 | First robot's link angle with respect to vertical |
| θ_2 | Second robot's link angle with respect to vertical |
| $\theta_{LL1}, \theta_{LL2}$ | Angles between L- LL1 and L-LL2 |
| θ_{opt} | Angle between L and R |
| θ_R | The angle between both bearings |
| <i>Subscript</i> | |
| A | Ankle |
| H | Hip |
| K | Knee |
| t | Trunk |
| p | Pelvis |
| L | Left |
| R | Right |

Appendix 1: Human model equations of motion

In this section, the EoMs of all human limbs are represented.

Ankle

$$\begin{aligned} X - \text{direction} : F_{x_A} + F_x &= m_f \ddot{x}_f \\ Z - \text{direction} : F_{z_A} + F_z - m_f g &= m_f \ddot{z}_f \end{aligned} \quad (36)$$

$$\begin{aligned} T_A + M - F_x L_{\text{contact}} \cos(\theta_p + \theta_H + \theta_K + \theta_A - \theta_{\text{contact}}) + \\ + F_z L_{\text{contact}} \sin(\theta_p + \theta_H + \theta_K + \theta_A - \theta_{\text{contact}}) - \\ - m_f g L_{f-\text{CoG}} \sin(\theta_p + \theta_H + \theta_K + \theta_A - \theta_{\text{contact}}) = \\ \bar{I}_f (\ddot{\theta}_p + \ddot{\theta}_H + \ddot{\theta}_K + \ddot{\theta}_A) + \\ + m_f \ddot{z}_f L_{f-\text{CoG}} \sin(\theta_p + \theta_H + \theta_K + \theta_A - \theta_{f-\text{CoG}}) - \\ - m_f \ddot{x}_f L_{f-\text{CoG}} \cos(\theta_p + \theta_H + \theta_K + \theta_A - \theta_{f-\text{CoG}}) \end{aligned} \quad (37)$$

Where θ_{contact} and L_{contact} represent the angle and distance of point of contact with respect to the ankle. Other parameters are illustrated in Figure 22.

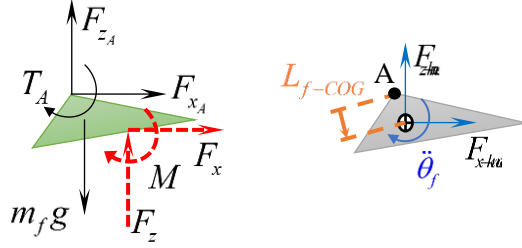


Figure 22. Foot FBD and kinematic diagram

Knee

$$\begin{aligned} X - \text{direction} : F_{x_K} - F_{x_A} &= m_s \ddot{x}_s \\ Z - \text{direction} : F_{z_K} - F_{z_A} - m_s g &= m_s \ddot{z}_s \end{aligned} \quad (38)$$

$$\begin{aligned} T_K - T_A - m_s g L_4 \sin(\theta_p + \theta_H + \theta_K) - \\ - F_{z_A} L_s \sin(\theta_p + \theta_H + \theta_K) + F_{x_A} L_s \cos(\theta_p + \theta_H + \theta_K) = \\ = m_s \ddot{z}_s L_4 \sin(\theta_p + \theta_H + \theta_K) - \\ - m_s \ddot{x}_s L_4 \cos(\theta_p + \theta_H + \theta_K) + \bar{I}_s (\ddot{\theta}_p + \ddot{\theta}_H + \ddot{\theta}_K) \end{aligned} \quad (39)$$

All parameters of the shank are depicted in Figure 23 as follow.

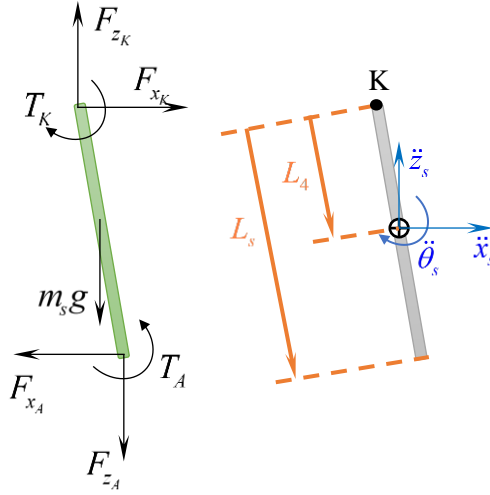


Figure 23. Shank FBD and kinematic diagram

Thigh

$$X - \text{direction} : F_{x_H} - F_{x_K} = m_{th} \ddot{x}_{th} \quad (40)$$

$$Z - \text{direction} : F_{z_H} - F_{z_K} - m_{th} g = m_{th} \ddot{z}_{th}$$

$$\begin{aligned} & T_H - T_K - m_{th} g L_3 \sin(\theta_p + \theta_H) - \\ & F_{z_K} L_{th} \sin(\theta_p + \theta_H) + F_{x_K} L_{th} \cos(\theta_p + \theta_H) = \\ & = m_{th} \ddot{z}_{th} L_3 \sin(\theta_p + \theta_H) - \\ & - m_{th} \ddot{x}_{th} L_3 \cos(\theta_p + \theta_H) + \bar{I}_{th} (\ddot{\theta}_p + \ddot{\theta}_H) \end{aligned} \quad (41)$$

where \bar{I}_{th} is thigh moment of inertia about thigh's CoG. Other parameters are illustrated in Figure 24 as follow.

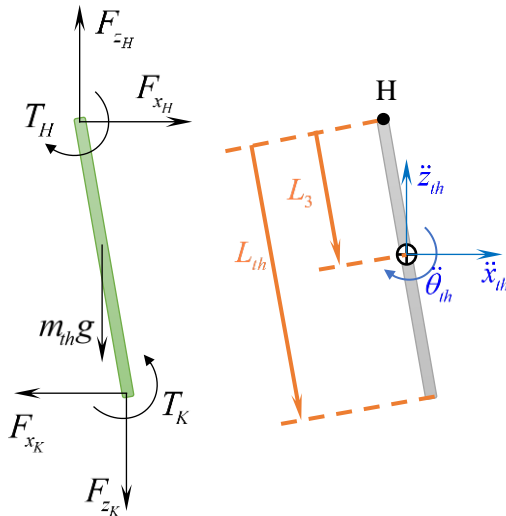


Figure 24. Thigh FBD and kinematic diagram

Trunk

$$\begin{aligned}
X - \text{direction} : F_{x_t} &= m_t \ddot{x}_t \\
Z - \text{direction} : F_{z_t} - m_t g &= m_t \ddot{z}_t
\end{aligned} \tag{42}$$

$$\begin{aligned}
T_t + m_t g L_2 \sin(\theta_p + \theta_t) &= m_t \ddot{x}_t L_2 \cos(\theta_p + \theta_t) - \\
&- m_t \ddot{z}_t L_2 \sin(\theta_p + \theta_t) + \bar{I}_{th} (\ddot{\theta}_p + \ddot{\theta}_t)
\end{aligned} \tag{43}$$

All the parameters of this equation are shown in Figure 25.

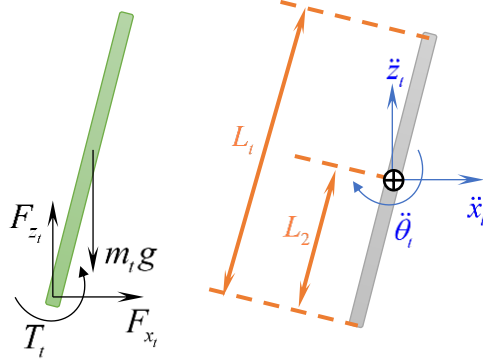


Figure 25. Trunk FBD and kinematic diagram

Pelvis

$$\begin{aligned}
X - \text{direction} : F_{x_p} - F_{x_t} - (F_{x_{HR}} + F_{x_{HL}}) &= m_p \ddot{x}_p \\
Z - \text{direction} : F_{z_p} - F_{z_t} - (F_{z_{HR}} + F_{z_{HL}}) - m_p g &= m_p \ddot{z}_p
\end{aligned} \tag{44}$$

$$\begin{aligned}
T_p &= T_t + T_{HR} + T_{HL} - \\
&- (F_{x_{HR}} + F_{x_{HL}}) L_{11} \cos(\theta_p) + (F_{z_{HR}} + F_{z_{HL}}) L_{11} \sin(\theta_p) - \\
&- F_{z_t} L_1 \sin(\theta_p) + F_{x_t} L_1 \cos(\theta_p) + \bar{I} \ddot{\theta}_p
\end{aligned} \tag{45}$$

All the forces and parameters of these equations are depicted in Figure 26.

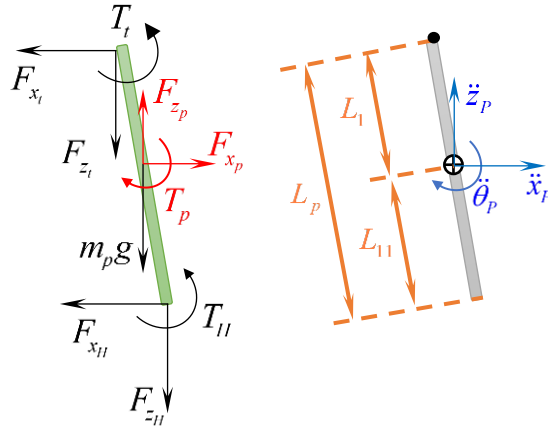


Figure 26. Pelvis FBD and kinematic diagram

Where F_{x_p} , F_{z_p} and T_p are virtual forces acting on virtual pelvis joint.